

Marginal speed confinement resolves the conflict between correlation and control in natural flocks of birds

Andrea Cavagna^{1,2}, Antonio Culla^{*,2,1}, Xiao Feng^{1,2}, Irene Giardina^{2,1,3}, Tomas S. Grigera^{4,5,6}, Willow Kion-Crosby^{1,2}, Stefania Melillo^{1,2}, Giulia Pisegna^{2,1}, Lorena Postiglione^{1,2}, Pablo Villegas^{1,2}

¹ *Istituto Sistemi Complessi, Consiglio Nazionale delle Ricerche, UOS Sapienza, 00185 Rome, Italy*

² *Dipartimento di Fisica, Università Sapienza, 00185 Rome, Italy*

³ *INFN, Unità di Roma 1, 00185 Rome, Italy*

⁴ *Instituto de Física de Líquidos y Sistemas Biológicos CONICET - Universidad Nacional de La Plata, La Plata, Argentina*

⁵ *CCT CONICET La Plata, Consejo Nacional de Investigaciones Científicas y Técnicas, Argentina and*

⁶ *Departamento de Física, Facultad de Ciencias Exactas, Universidad Nacional de La Plata, Argentina*

Speed fluctuations of individual birds within natural flocks are moderate, due to the aerodynamic, energetic and biomechanical constraints of flight. Yet the spatial correlations of such fluctuations are scale-free, namely they have a range as wide as the entire group. Scale-free correlations and limited fluctuations set conflicting constraints on the mechanism controlling the speed of each bird, as the factors boosting correlations tend to amplify fluctuations, and vice versa. Here, using a field-theoretical approach, we demonstrate that a marginal speed confinement that ignores small deviations from the natural reference value while ferociously suppressing larger fluctuations, is the only mechanism reconciling scale-free correlations with biologically acceptable flocks' speed, a result that we confirm through numerical simulations of self-propelled particles in three dimensions. We validate the theoretical as well as the numerical predictions of this analysis by comparing our results with field experimental data on starling flocks having group sizes spanning an unprecedented interval of over two orders of magnitude.

Since the early stages of the effort to formulate a mathematical description of flocking behaviour, the fundamental dynamical rule common to all theoretical models has been that of local mutual imitation: each individual within the group tends to adjust its state of motion to that of its neighbours [1–8]. This type of imitative behaviour can be either explicitly prescribed by the model through a direct interaction between the animals' velocities [1, 3–5], or it may be an effective interaction emerging from simpler positional rules, as attraction and repulsion [2, 7–9], depending on the coarse-graining level we decide to work at. In either case, effective imitation of the local neighbours is the cornerstone of organised flocking dynamics. The early models also assumed that all individuals within the group moved with the same constant speed [1–6]. In that case, mutual imitation requires each particle to only adapt the orientation of its velocity to that of its neighbours. In real flocks, however, the individual speeds fluctuate [10], hence mutual imitation requires a bird to also adjust its speed to that of its neighbours. In contrast to orientation, though, speed control cannot be left just to mutual imitation, as nothing then would prevent birds to move in sync at unreasonably large (or small) speeds. One therefore needs to devise a control mechanism aimed at keeping the individual speed of each bird in the ballpark of some reference biological value, v_0 , set by species-specific aerodynamic and biomechanical constraints [11].

The most straightforward way to confine the individual speeds is through a *linear* restoring force: whenever

the speed v_i of particle i deviates from the natural reference value v_0 , it gets 'pushed back' proportionally to the deviation. Linear speed control is widely used to study the collective behaviour of the most diverse systems, as bird flocks [12, 13], fish schools [14], pedestrian collectives [15–17], robots swarms [18], and vehicle crowds [19], to name just a few examples. Linear control also captures a crucial experimental trait of bird flocks, namely the fact that speed correlations are scale-free [10]: when the stiffness of the linear force is small enough, the correlation length grows linearly with the group's size, as it happens in real flocks [12], thus ensuring that group fragmentation is very low [13]. Linear speed control therefore lies at the basis of all current theories of collective behaviour.

Here, by using field data on starling flocks, numerical simulations of self-propelled particles and statistical field theory, we will prove that linear speed confinement entails an intrinsic conflict between scale-free correlations and group's speed control, which is impossible to resolve. Such conflict has not been uncovered until now, due to the lack of experimental data on animal groups with a wide-enough size spectrum. At its core, the problem is that, to reproduce long-range correlations, linear control requires a weak speed-confining force, so that the animal's speed is very loosely confined around its reference value, v_0 . When this happens, entropic forces push the typical speed of the group to grow unreasonably larger than the reference natural speed, thus completely destroying the agreement between theory and experiments. We will show that, to resolve this conflict, quite a different speed control mechanism is needed.

Experimental evidence from field observations

We consider 3D experimental data on natural flocks of

*Corresponding author, e-mail: a.culla@uniroma1.it

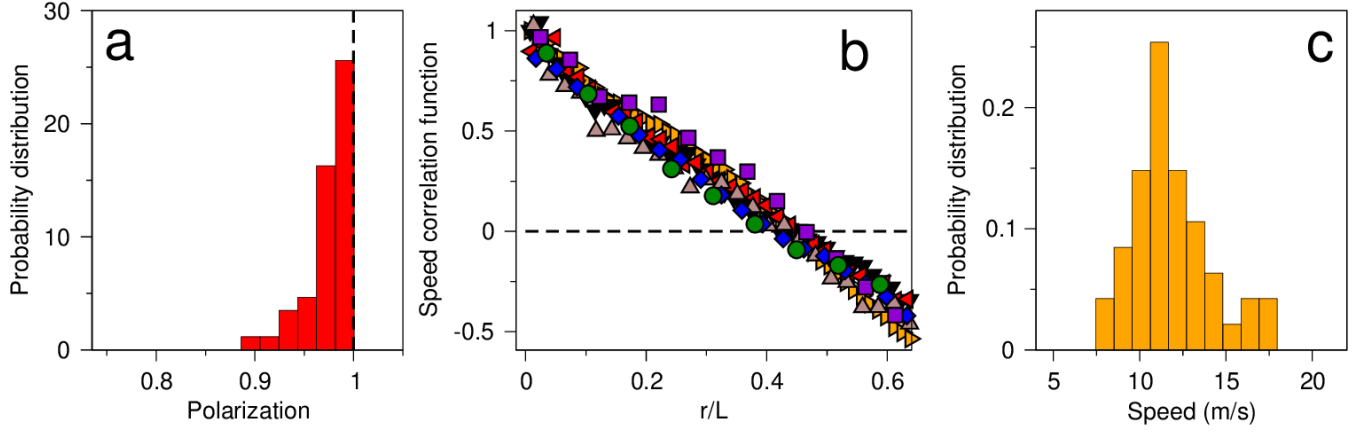


FIG. 1: **Experimental evidence on starling flocks.** **a:** Probability distribution of the polarization, $\Phi = (1/N) \sum_i \mathbf{v}_i / v_i$ across all recorded flocks; data clearly indicate that these are highly ordered systems, incompatible with the standard notion of near-criticality. **b:** The equal-time space correlation function of the speed fluctuations (for the precise definition of the correlation function see Methods), plotted against the distance r between the birds rescaled by the flock's size L , for some typical flocks; the fact that all the curves collapse onto each other indicates that the spatial range of the speed correlation, namely the correlation length ξ_{sp} , scales with L , i.e. that the system is scale-free (see also Fig.2a and Fig.2c). **c:** Probability distribution of the mean speed of birds within a flock, $s = (1/N) \sum_i v_i$, across all recorded flocks. The average mean speed is 11.9 m/s, with typical fluctuations of 2.3 m/s.

starlings (*Sturnus vulgaris*) in the field. To the data previously reported by our lab in [20–22], we added new data from our most recent campaign of acquisition conducted in 2019-2020 (see Methods for details of the experiments, and Table S1 in the SI for all biological data in each acquisition). The new data expand the span of the group sizes between $N = 10$ and $N = 3000$ animals, a wider interval than any previously reported study. As we shall see, this will be crucial in selecting the correct theory.

The three main experimental results that are of interest for us here are the following: *i)* Flocks are highly ordered systems. The polarization, $\Phi = (1/N) \sum_i \mathbf{v}_i / v_i$ (where N is the total number of birds in the flock, \mathbf{v}_i is the vector velocity of bird i , and v_i is its modulus, i.e. speed), is always quite large, typically above 0.9 (Fig.1a). This observation rules out the possibility that flocks are close to an ordering transition, hence near-criticality in the standard ferromagnetic sense cannot be invoked to explain the phenomenology of flocks. Instead, these are clearly systems deep into their ordered phase. *ii)* Speed fluctuations are correlated over long distances, namely their spatial correlation functions are scale-free (Fig.1b) [10]. Having ruled out standard near-criticality because of the previous point, the origin of this trait is puzzling. Unlike the case of orientations, scale-free correlations of the speed cannot be explained as the effect of spontaneously breaking a continuous symmetry [23]; in fact, in standard statistical physics systems fluctuations of the modulus of the order parameter are heavily suppressed in the ordered phase, so they are very much short-range correlated [24]. *iii)* Flock-to-flock speed fluctuations are moderate (Fig.1c). The average cruising speed of starlings within a flock is about 12 meters-per-

second (m/s), with typical fluctuations of 2 m/s [10]. This is also the typical cruising speed of an entire flock, namely $s = (1/N) \sum_i v_i$, whose distribution is reported in (Fig.1c). Hence, neither the individuals, nor the group, ever cruise at a speed much different from the natural reference value, v_0 . As we shall see, this seemingly puny experimental trait may become tremendously difficult to reconcile with scale-free correlations at the theoretical level.

General theory

The reference flocking dynamics we will consider here is the Vicsek model [4, 25, 26], in which the animals' velocities interact through an explicit velocity coupling, aimed at describing the effective imitation between neighbouring individuals. This kind of dynamics can be written in a compact way as follows,

$$\frac{d\mathbf{v}_i}{dt} = -\frac{\partial H}{\partial \mathbf{v}_i} + \boldsymbol{\eta}_i \quad (1)$$

$$\frac{d\mathbf{x}_i}{dt} = \mathbf{v}_i, \quad (2)$$

where $\boldsymbol{\eta}_i$ is a white noise with strength proportional to T , a parameter playing the role of an effective temperature in the statistical physics context, namely $\langle \boldsymbol{\eta}_i(t) \boldsymbol{\eta}_j(t') \rangle = 2dT\delta_{ij}\delta(t-t')$; H is a cost function (or effective Hamiltonian), whose derivative with respect to \mathbf{v}_i represents the social force acting on the particle's velocity.¹ At a fairly

¹ The effective friction coefficient in front of $\dot{\mathbf{v}}_i$ in (1) can be set to 1 through an appropriate rescaling of time [27].

general level, we can write,

$$H = \frac{1}{2}J \sum_{i,j}^N n_{ij}(\mathbf{v}_i - \mathbf{v}_j)^2 + \sum_i^N V(\mathbf{v}_i), \quad (3)$$

where the first term represents the imitation interaction between particles' velocities, having strength J , and the second term is the speed control term, which affects each particle independently. The adjacency matrix, n_{ij} , is 1 for interacting neighbours and 0 otherwise. The self-propulsion part of the dynamics, (2), implies that the interaction network depends on time, $n_{ij} = n_{ij}(t)$. In the original Vicsek model the speed of the particles is kept constant, $|\mathbf{v}_i| = v_0$. Here we want to study speed fluctuations and their correlations, hence we relax the hard Vicsek constraint and use the confining potential, $V(\mathbf{v}_i)$, to keep the speed of each particle confined around the natural reference value, v_0 . Note that the actual speed of a bird will be the product of the interplay between the individual confining force and the collective imitation among the birds.

Linear speed control

The simplest control, and indeed the one used in virtually all models with fluctuating speed to date, consists of a Gaussian potential confining the speed,

$$V(\mathbf{v}_i) = g(v_i - v_0)^2, \quad (4)$$

where $v_i = |\mathbf{v}_i|$. This potential generates a linear restoring force acting on the speed in the equation of motion (1), hence it is called *linear speed control*. The constant g is the stiffness of the restoring force, and it can be interpreted as the elastic constant of a spring keeping the speed around its natural reference value, v_0 . The determination of the correlation length ξ_{sp} of speed fluctuations in the case of a linear speed control has been worked out in [12],

$$\xi_{sp} = r_1 \left(\frac{Jn_c}{g} \right)^{1/2}, \quad (5)$$

where r_1 is the mean inter-particle distance and n_c is average number of interacting nearest-neighbours. The explanation of (S21) is simple: the theory defined by (3) and (4), has a critical point at $g = 0$, where the correlation length diverges. Conversely, large values of the speed stiffness g suppress the range of speed correlations [12]. To have scale-free correlations with linear control, then, it is sufficient to have $\xi_{sp} \gg L_{\max}$ (where L_{\max} is the size of the largest flock in the dataset), that is the stiffness g must be smaller than $1/L_{\max}^2$ (see the SI for more details on the bounds on g in the linear theory).

This theoretical scenario is confirmed in Fig.2a, where we report the correlation length of the speed fluctuations, ξ_{sp} , vs the system's size, L , in numerical simulations of self-propelled particles (SPP) regulated by linear speed control (colored points - see Methods and SI for

details of the SPP simulations): when the speed stiffness g is small enough, namely smaller than $1/L_{\max}^2$, the correlation length ξ_{sp} correctly scales linearly with L over the whole range (dark red points), thus reproducing the scale-free nature of the experimental correlation length (black points). On the contrary, if g is larger than $1/L_{\max}^2$, the range of the correlation grows linearly with L only up to a certain size, and then it saturates to its bulk value (S21) (orange and yellow points). We conclude that, if correlations were our only experimental concern - as it has been the case in the literature up to now - there would be no need to increase the speed stiffness g beyond $1/L_{\max}^2$, and everything would be fine.

However, when we consider as an observable the mean speed of the flock, $s = (1/N) \sum_i v_i$, the outlook for the linear theory gets bleak. Empirical data show that the mean speed does not change much from flock to flock and it does not have any dependence on the flock's number of birds, N (black points in Fig.2b). Let us see what is the prediction of the linear theory for the mean speed, s . Calculating the probability distribution, $P(s)$, from equations (1)-(2) is a prohibitive task, due to the time-dependence of the interaction network, $n_{ij}(t)$; however, previous studies have shown that, in the deeply ordered phase in which flocks live, the timescale for rearrangement of $n_{ij}(t)$ is significantly larger than the relaxation time of the velocities, hence one obtains reasonably accurate results by assuming a time-independent form of n_{ij} , namely a fixed interaction network [28]; as we shall see from the perfect agreement between off-equilibrium SPP simulations and theory, this approximation works very well. Under this assumption (plus some more bland algebraic approximations - see SI for details) one can calculate the probability distribution of the mean speed, obtains for $d = 3$ the result,

$$P(s) = \frac{1}{Z} s^2 \exp \left[-\frac{Ng}{T} (s - v_0)^2 \right], \quad (6)$$

where Z is a normalization factor. We can easily evaluate the peak of this distribution, that is the typical value of the mean speed,

$$s_{\text{typical}} = \frac{1}{2}v_0 \left(1 + \sqrt{1 + \frac{4T}{Ngv_0^2}} \right). \quad (7)$$

For $N \rightarrow \infty$ we get $s_{\text{typical}} = v_0$, so all is good for infinitely large flocks, as their typical speed is just the same as the natural reference speed, v_0 . But in finite groups serious troubles emerge, as the typical speed *grows* for decreasing N , eventually becoming absurdly larger than the natural reference value, v_0 ; and because in (7) the combination Ng appears, this disastrous effect is all the more serious the smaller the speed stiffness g , so that for very weak control, even relatively large flocks will have a biologically implausible speed. Yet weak control g is exactly what we need to grant strong correlations! Hence linear control has a serious problem.

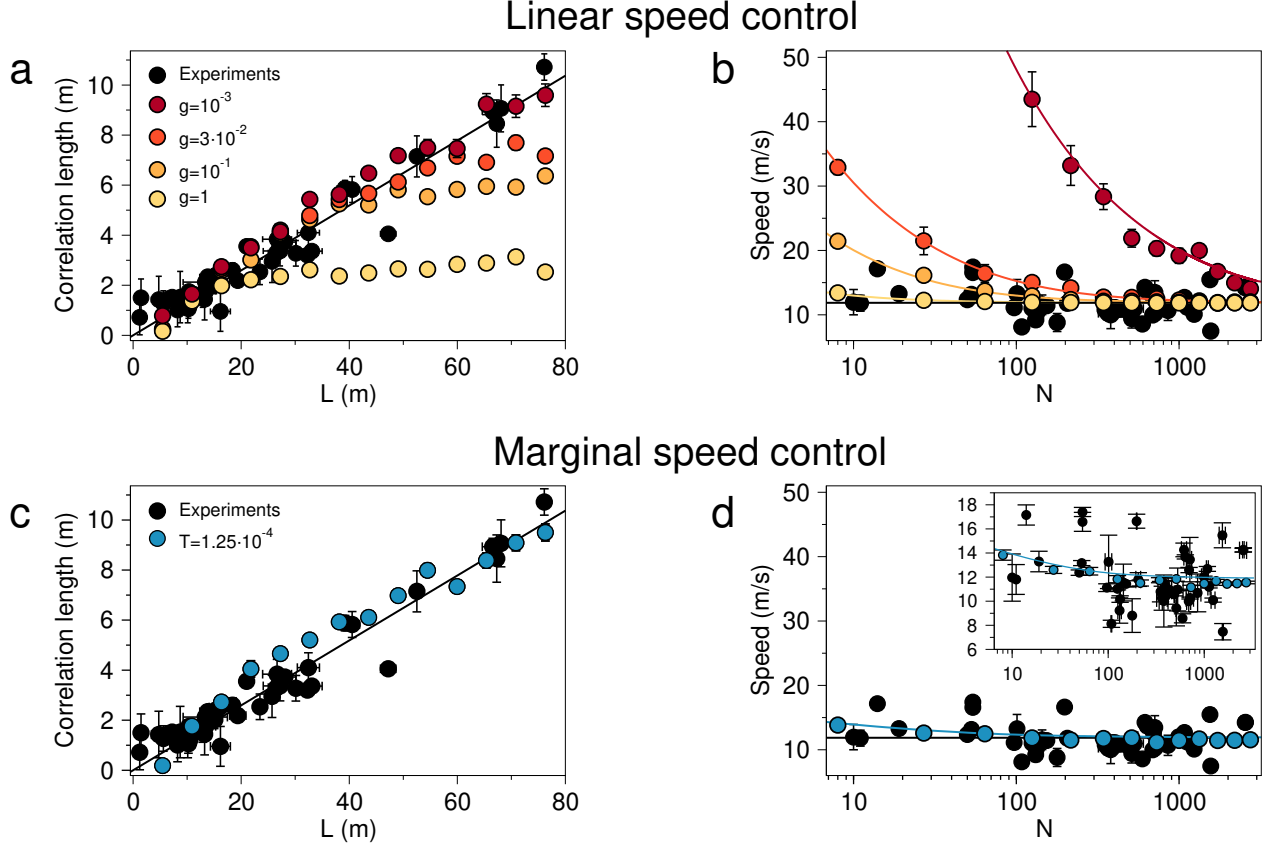


FIG. 2: Linear vs Marginal speed control. **a:** Natural flocks show a clear scale-free behaviour of the speed correlation length, ξ_{sp} , which scales linearly with L (Pearson coefficient $r_P = 0.97$, $p < 10^{-9}$). SPP simulations with linear speed control yields scale-free correlations over the entire range of L only at the *smallest* value of the stiffness g (dark red). **b:** Natural flocks show no detectable dependence of their mean speed on the number of birds in the flock (Spearman coefficient $r_S = -0.13$, $p = 0.21$; the black line is the average over all flocks). SPP simulations with linear control give a near-constant speed compatible with experiments only at the *largest* value of the stiffness g (light yellow); coloured lines represent the theoretical prediction of (6). Linear speed control is therefore unable to reproduce both experimental traits at the same time. **c:** The correlation length in SPP simulations with marginal speed control scales linearly with L over the full range, provided that the temperature/noise T is low enough to have a polarization equal to the experimental one. **d:** At the *same* value of the parameters as in panel c, SPP simulations with marginal control give mean group's speed very weakly dependent on N , fully compatible with the experimental data; the blue line represents the theoretical prediction of (S27). Inset: same data over a smaller range to appreciate the agreement between theory and simulations. (Numerical and experimental correlation lengths are reported on the same scale by matching the curves at the scale-free value of the parameters; numerical and experimental speeds are reported on the same scale by matching the curves at the largest value of N . Colored points correspond to averages over numerical data, error bars to standard deviations. Black points correspond to the median (over time) of experimental data for each individual flocking event, error bars to median absolute deviations.)

The physical reason for this drift of the mean speed in the linear theory is the following. In absence of the prefactor s^2 in the distribution (6), a decrease of the stiffness g would increase the flock-to-flock fluctuations of the mean speed, but its typical value would be always equal to the natural one, namely v_0 . The s^2 prefactor, though, changes this, pushing the maximum of the distribution at larger and larger speed for decreasing g . Where is this prefactor from? It is essentially the Jacobian of the change of variable between the d -dimensional velocity vector and the modulus of the ve-

locity (see SI); in generic dimension, $s^{d-1}ds$ is the volume in phase space of all configurations with the same mean speed, but variable velocity direction (an identical term appears in the Maxwell-Boltzmann speed distribution). This is an *entropic* term, which boosts the probability of large speed merely because there are more ways to realise larger rather than smaller velocity vectors. When the imitation force is strong (as it is within a flock) and the speed-confining force is weak (as it must be for the sake of scale-free correlation), the system is allowed to gain entropy by increasing in a coordinated fashion *all*

the individual speeds of the particles; as this entropic push is not suppressed by a strong enough exponential weight, it gives rise to unreasonably fast flocks.

This theoretical prediction - and its disastrous consequences - are confirmed by a comparison between numerical SPP simulations ruled by linear speed control and experimental data. Fig. 2b shows that, once the reference speeds v_0 of the theory and of the experiments are matched at the largest sizes, for small values of N and g numerical flocks with linear speed control (dark red points) have a mean speed that is *completely incompatible* with that of actual experimental flocks (black points), which shows no appreciable dependence on N . To contrast the increase of the typical mean speed in smaller SPP flocks one needs a larger value of the speed stiffness g (light yellow points), but we know from the previous discussion that this depresses the range of the speed correlations, so that one fails to reproduce scale-free correlations, Fig. 2a. This is the blanket-too-short dilemma of linear speed control: either we use a speed stiffness g small enough to reproduce scale-free correlations even at the largest observed values of N , but in that case we get implausible large speed at low N (dark red points), or we increase g to tame the entropic boost of the speed and keep it within the experimental fluctuations at low N , but then we lose scale-free correlations at large N (light yellow points). Linear speed control cannot yield both experimental traits at the same time. We must therefore turn to some other mechanism.

Marginal speed control

In statistical physics, the correlation length ξ is connected to the inverse of the quadratic curvature of the (renormalized) potential, calculated at its minimum [29–31]; very small curvature implies very large correlation length, so that a divergent ξ is always due to a zero second derivative (or marginal mode) along some direction of the (renormalized) potential. This is also the case for linear speed control (4): the second derivative of the quadratic potential along the speed is proportional to g , hence when g is small, the correlation length is large. The problem, however, is that because the function is quadratic, by decreasing g we weaken the *whole* potential confining the speed, not just its curvature, hence giving a freeway to the entropic boost we have discussed before, ultimately resulting in an implausible large speed of small flocks.

This state of affairs suggests that we must turn to a confining potential that *does not* vanish entirely when its curvature does. To find this potential we proceed through general considerations of symmetry and common sense. First, the potential must keep the speed around the reference natural value v_0 and it must diverge for large values of the speed; secondly, it must be rotationally symmetric in the whole velocity vector; third, it must have the simplest mathematical form compatible with the previous conditions and with the experimental evidence. The most general form of a rotationally symmetric potential that

confines the speed around the natural reference value v_0 is, $V(\mathbf{v}_i) = (\mathbf{v}_i \cdot \mathbf{v}_i - v_0^2)^p$, where the integer power $p \geq 2$ must be even, in order to produce a minimum of the potential at v_0 . For $p = 2$ we have the classic $O(n)$ potential of standard vector ferromagnets [24, 29]; this theory is not suitable for our purposes, though, as in the low-temperature symmetry-broken phase it cannot develop zero curvature in the speed direction *unless* we put an amplitude g in front of the whole potential and let g itself go to zero; but this is what we already did for the Gaussian case, and we know it does not work.² Indeed, for $p = 2$ and for $v_i \sim v_0$, we can write, $V \sim (v_i - v_0)^2$, which is nothing else than the Gaussian potential that we already took into consideration.³

The next simplest possibility is $p = 4$, which gives the following speed-control potential,

$$V(\mathbf{v}_i) = \frac{1}{v_0^6} \lambda (\mathbf{v}_i \cdot \mathbf{v}_i - v_0^2)^4 \quad (8)$$

where, thanks to the v_0^{-6} normalization, the amplitude λ has the same physical dimensions as the other coupling constants, J and g . This potential was first studied on purely speculative grounds in [35], although no SPP simulations, nor comparison with the experiments, were performed there. The crucial feature of the potential in (8) is that its second derivative with respect to the speed is *always zero*, irrespective of the value of the amplitude λ , hence we will call this *marginal speed control*. Higher order powers in the expansion of the potential are nonzero and very steep, though, thus confining the speed much more effectively to its reference value, v_0 , compared to linear control. Correspondingly, the speed-restoring force is very weak for small deviations from v_0 , but very strong for large deviations (we will discuss later about the biological plausibility of this kind of nonlinear speed confinement).

The complete absence of a quadratic term in the expansion of (8) seems to suggest that the marginal potential gives rise to an infinite correlation length of speed fluctuations under all physical conditions; in fact, this is not the case. Speed correlations are regulated by the confining potential (i.e. the energy), but also by the fluctuations induced by the noise (i.e. the entropy): at very low noise the marginal potential dominates, so that speed fluctuations are indeed scale-free, while by increasing the noise the correlation is increasingly suppressed by entropic fluctuations [35]. In field theory terms, what happens is that

² Modulus fluctuations in the standard $O(n)$ theory are different from longitudinal fluctuations; the latter, being coupled to the massless transverse fluctuations, are also scale-free (albeit with a weaker divergence), while the former are truly massive fluctuations, hence they have finite (in fact very small) correlation length and susceptibility [32–34].

³ The fact that the ‘linear’ speed control theory is essentially identical to the standard $O(n)$ model, shows that that theory is not ‘linear’ at all, nor Gaussian, in the actual degrees of freedom, v_i .

at finite temperature entropy provides a non-zero second derivative of the renormalized potential, i.e. a non-zero mass of speed fluctuations, and therefore a finite correlation length. The mass goes to zero at $T = 0$, where the speed correlation length diverges. As a consequence, the marginal theory has a zero-temperature (or zero-noise) critical point, where the correlation length of the speed fluctuations diverges. A mean-field analysis [35] shows that the speed correlation length diverges as,

$$\xi_{\text{sp}} \sim \frac{1}{T^{1/2}}, \quad (9)$$

where the generalized temperature T is the strength of the noise in (1). This scenario has an interesting and very convenient consequence: in the marginal theory, by simply decreasing the noise strength T , we bring home two out of three empirical traits, that is a large polarization *and* a large correlation length, a somewhat unusual result within standard statistical systems. But what about the constraint of having a biologically reasonable group speed?

The calculation of the distribution of the mean speed of flocks under the marginal potential is more complicated than in the linear case (see SI), but under some reasonable approximations one obtains,

$$P(s) = \frac{1}{Z} s^2 \exp \left[-\frac{N\lambda}{Tv_0^6} (v_0^2 - s^2)^4 \right] \quad (10)$$

which has two great differences compared to the linear case: first, the power 4 in the exponential tames the entropic push of the s^2 term extremely sharply; secondly, the amplitude λ , unlike g , does *not* need to be small to grant scale-free correlations, so the exponential weight remains always effective in suppressing large values of the mean speed, s . The maximum of this distribution, i.e. the typical mean speed of the flock, is given by (see SI for details),

$$s_{\text{typical}} \simeq \begin{cases} v_0 & \text{for } N \gg \frac{T}{\lambda v_0^2} \\ v_0 \left(\frac{T}{4N\lambda v_0^2} \right)^{1/8} & \text{for } N \ll \frac{T}{\lambda v_0^2} \end{cases}$$

As in the linear case, for $N \rightarrow \infty$, the typical speed of the flocks becomes the same as the natural reference speed, v_0 , while it increases for smaller sizes. However, in the marginal case this growth is very moderate indeed: the strength T of the noise is small (to have large correlation length) and the amplitude λ is finite, so that the crossover size $N = T/(\lambda v_0^2)$, below which the mean speed increases, is very small, thus shielding this regime; moreover, the exponent of the speed's increase for small N is $1/8$, significantly smaller than the exponent $1/2$ of linear speed control (see equation (7)). For these two reasons marginal speed control is so much more effective than linear control at small N .

These theoretical results are fully confirmed by numerical simulations of SPP flocks regulated by marginal speed control (Fig.2c and Fig.2d). Moreover, the comparison

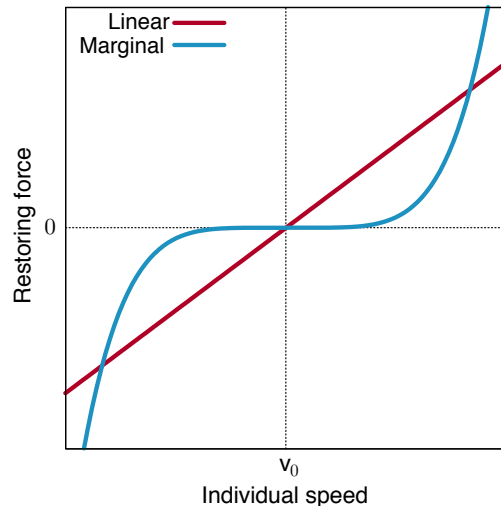


FIG. 3: **Qualitative sketch of linear vs marginal speed-restoring force.** In the linear case the force pulls the speed back to its natural reference value v_0 proportionally to the deviation from v_0 . Instead, in the marginal case, the force is extremely weak for small deviations from the reference speed, while it increases very sharply for large deviations, harshly suppressing them.

with experimental data on real starling flocks in the field indicates that marginal control is indeed the right way to go, as with just *one* reasonable set of parameters - the only crucial one in fact being the low noise strength, T - numerical simulation of SPP flocks with marginal speed control reproduce the experimental data very well: the correlation length ξ_{sp} scales linearly with L up to the largest size (Fig.2c), and the mean speed s shows only a very moderate increase at low N , well within the scatter of the empirical data (Fig.2d). We stress once again that all three pieces of phenomenology - large polarization, large correlation length, moderate speed at all group sizes - are achieved by marginal control by doing just one very sensible thing, namely pushing the system into the ordered phase real flocks naturally belong to. The entropy-triggered conflict between scale-free correlation and moderate group speed that hinders linear control is therefore completely resolved by the marginal theory.

Biological significance

What is the biological meaning of marginal speed control in the context of avian flight? The highly non-linear marginal potential (8) implies that small speed fluctuations elicit nearly zero restoring force, while larger speed fluctuations are pushed back extremely sharply, in contrast with the constant slope of a linear confining force, Fig.3. Is this reasonable for actual birds in a flock? Small speed fluctuations are certainly not prevented by biomechanical constraints, but they could be depressed by energetic expenditure concerns, as changing the speed requires extra energy consumption; however, starlings

prove to be *very* liberal about their energy expenditure habits while flocking [36–38]: although their metabolic rate is dramatically higher in flight than on the roost [36], these birds will spectacularly wheel every day for half an hour before landing, expending energy at a ferocious rate; this suggests that small extra energy expenditures due to small speed fluctuations may indeed be weaker-than-linearly suppressed. On the other hand, large speed fluctuations clash against biomechanical and aerodynamic constraints, which are set very stringently by anatomy, physiology and physics [39–41]; therefore, a stronger-than-linear suppression of large speed fluctuations also seems quite reasonable. In view of the general nature of this argument, it seems to us that marginal speed control may not only be a fairly natural mechanism from a biological point of view, but also quite a general one, possibly extending beyond the case study of starling flocks.

Methods

Experiments. Empirical observations of starling flocks have been performed in Rome, from the terrace of Palazzo Massimo alle Terme, in front of a large roosting site at the Termini Railway Station. The experimental technique used is stereoscopic photography, where multiple synchronized video-sequences of a flocking event are acquired from different observation points with a calibrated multi-camera video-acquisition system [42]. Digital images are then analysed with a specifically designed tracking software [43], in order to extract from the raw data the three-dimensional trajectories of the individual birds in the flock.

Data have been collected across the years during several experimental campaigns. The very first data were collected in the context of the *Starflag* project [20, 21], between 2007 and 2010, using Canon D1-Mark II cameras, shooting interlaced at 10 frames-per-second (FPS), with a resolution of 8.2 Megapixels (MP). A second campaign took place between 2011 and 2012, using faster cameras, namely IDT M5, shooting at 170FPS with a resolution of 5MP. A final campaign took place in the last months of 2019 and in January and February 2020. This campaign uses state-of-the-art IDT OS10-4K cameras, shooting at 155FPS with a resolution of 9.2MP. Overall, we have data from flocks with sizes ranging between 10 and 2500 birds, a span that is essential to differentiate between linear and marginal speed control.

All campaigns have been conducted with a three camera system exploiting trifocal geometry [44]. The image analysis - segmentation of individual birds, stereometric matching and dynamical tracking - have been performed using the method of [20, 21] for the first campaign, and the most advanced method of [43] for the second and third campaigns. We summarise in Table S1 in the SI all the experimental quantities used in our analysis for each

flocking event.

Correlation functions and correlation length. The speed spatial connected correlation function is defined as [45]

$$C(r) = \frac{\sum_{i,j}^N \delta v_i \delta v_j \delta(r - r_{ij})}{\sum_{i,j}^N \delta(r - r_{ij})} \quad (11)$$

where N is the number of individuals in the system, $r_{ij} = |\mathbf{r}_i - \mathbf{r}_j|$ is the mutual distance between individuals i and j , and

$$\delta v_i = v_i - \frac{1}{N} \sum_k^N v_k \quad (12)$$

is the fluctuation of the individual speed $v_i = |\mathbf{v}_i|$ with respect to the mean speed of the group $s = (1/N) \sum_i v_i$, evaluated at a given instant of time. The function $C(r)$ represents the instantaneous average of mutual correlations among all pairs at distance r : in systems with local, distance-dependent interactions, for large enough system sizes, this quantity is a good proxy of the typical correlation at that distance, as computed with the correct theoretical measure. A full discussion of definition (11), its asymptotic limit, finite size effects, and behaviour in known cases, can be found in [45]. Here we notice that the correlation function (11) is the only possible definition applicable to experimental data, where no a priori information is available on the true nature of the dynamics. This definition has indeed been used in all the previous analysis of speed correlations mentioned in this paper. We display in Fig.S2 of the SI the correlation function (11) computed, respectively, from experimental data (panel a), and from numerical simulations with a linear speed control model (panel b) and a marginal speed control model (panel c).

For each configuration of the system (at a given time) we estimate the correlation length as:

$$\xi = \frac{\int_0^{r_0} dr \, r \, C(r)}{\int_0^{r_0} dr \, C(r)} \quad (13)$$

and then we perform a time average of this quantity over different configurations. The point r_0 is the first point for which $C(r) = 0$. Such a point always exists due to the very definition of correlation function given in (11) (the integral of $C(r)$ between 0 and the size of the system L always vanishes). (13) provides a reliable estimate of the correlation length in every regime, both when the system is scale-free with long-range correlations and when the system is far from criticality with short-range correlations (in the linear speed control model we can see

all this phenomenology, simply by changing the parameter g , see Fig. 2a). The reason is that (13) makes use of the information encoded in the zero-crossing point r_0 , together with the shape of the entire function $C(r)$. When correlations are short-range and the correlation function is nearly exponential [45], e.g. $C(r) \sim e^{-r/\hat{\xi}}$, given that it almost vanishes after the point r_0 , we can think of extending the integrals of (13) up to L , and we obtain $\xi \sim \hat{\xi}$. Conversely, when correlations are long range, regardless of the precise shape of the $C(r)$, the first point of zero-crossing r_0 dominates, hence we obtain $\xi \sim r_0$. Other possible definitions are legitimate but, either they are reliable near criticality and they fail in the short-range correlation regime, or they capture the correlation range when it is much smaller than the system size, completely failing when the correlation range becomes extensive. For example, if one chooses r_0 as an estimate for the correlation length, it works efficiently when the system is scale-free, and r_0 identifies the size of the correlated domains, while it fails when the system has an intrinsic length-scale [10, 45]. On the other hand, in the phase of short-range correlations, it is easy to determine the correlation length via an exponential fit, because the $C(r)$ has an exponential shape [45]; however this procedure is unfeasible in the critical regime when the correlation functions do not have an exponential behaviour (see Fig. S2 in the SI).

Numerical simulations of SPP flocks. To investigate the flocking dynamics described by (1) and (2), we perform numerical simulations with a system of self-propelled particles. The flock is modeled as a set of particles moving in a three-dimensional space with update rules for positions and velocities, which are a discretized version of (1) and (2). Following a simple Euler integration scheme [46], we get

$$\mathbf{v}_i(t + \Delta t) = \mathbf{v}_i(t) + \Delta t \mathbf{F}_i + \delta \boldsymbol{\eta}_i \quad (14)$$

$$\mathbf{x}_i(t + \Delta t) = \mathbf{x}_i(t) + \Delta t \mathbf{v}_i(t) \quad (15)$$

Here the force $\mathbf{F}_i = \mathbf{F}_{int} + \mathbf{F}_{sc}$ acting on particle i contains both an alignment term \mathbf{F}_{int} ,

$$\mathbf{F}_{int} = -J \sum_j^N n_{ij}(t) (\mathbf{v}_i(t) - \mathbf{v}_j(t)) \quad (16)$$

and a speed control term \mathbf{F}_{sc} , which can be either linear:

$$\mathbf{F}_{sc} = 2g \frac{\mathbf{v}_i}{|\mathbf{v}_i|} (v_0 - |\mathbf{v}_i|) \quad (17)$$

or marginal,

$$\mathbf{F}_{sc} = \frac{8\lambda}{v_0^6} \mathbf{v}_i (v_0^2 - \mathbf{v}_i^2)^3 \quad (18)$$

The last term in (14) is a white gaussian noise with zero mean and variance:

$$\sigma_\eta^2 = 2dT\Delta t \quad (19)$$

where $d = 3$ is the space dimension and T is the effective temperature. The matrix $n_{ij}(t)$ is the adjacency matrix that defines which pairs interact; its entries can assume only the values 0 and 1, according to a rule of interaction that can be metric (i.e. $n_{ij} \neq 0$ if and only if $r_{ij} < r_c$) or topological (i.e. $n_{ij} \neq 0$ if j is one of i 's first n_c neighbours) [47, 48]. When working at fixed average density and in the very low temperature region where density fluctuations are small, there is not great difference between metric and topological interaction. Even though natural flocks are known to have topological interactions [47, 48], we therefore decide to perform simulations with the metric rule, which are much less expensive computationally. In this way, we are able to study systems in $d = 3$ with N up to 3×10^5 particles. We consider a metric connectivity matrix with interaction radius $r_c = 1.2$, such that the number of nearest neighbours at the time $t = 0$ is $n_c = 6$, close to the biological value [47, 48]. We then check a posteriori that the system remains spatially homogeneous in time by computing the distribution of the number of nearest neighbours for every simulation, and verifying that it is always sharply peaked around the initial value $n_c = 6$. All the simulations are made in a cubic box (of linear size L) with periodic boundary conditions. Individuals are initialized in a global polarized configuration on a cubic lattice with lattice spacing (i.e. nearest neighbour distance) $r_c = 1$ and then evolve off-lattice according to rules (14). The effective temperature clearly drives the system from a disordered to an ordered state through a phase transition at fixed density. However, since we are considering self-propelled particles, the same configurations can be reached using another control parameter defined as the ratio between the mean first neighbour distance r_1 , which directly depends on the density of the system, and the interaction radius r_c but at fixed noise. We decide to perform all the simulations at constant density $\rho = 1$, maintaining r_1/r_c constant and choosing the temperature according to the desired polarization.

We choose the value of the reference speed of the particles v_0 and of the integration step Δt to ensure an average displacement $\Delta r \simeq v_0 \Delta t$ much smaller than the size of the box L . In this way there is a weak rewiring of the interaction network during the time of simulation, consistently with the quasi-equilibrium condition of natural flocks [28]. The step of integration is selected as the maximum value granting a robust numerical integration in terms of errors and stationarity of the energy of the system (absence of trends in time or in size). In simulations with marginal speed control this algorithmic stability is achieved with $\Delta t = 0.01$, while linear speed control requires a $\Delta t = 0.001$. Every simulation consists in a run of length $N_{steps} = 2 \times 10^4$ steps for thermalization and in an independent run long $N_{steps} = 1.2 \times 10^6$ steps. From the latter we extract configurations every 1000 steps in order to compute the quantities needed by our analysis. In Table S2 of the SI we report the values of the other parameters used in the simulations.

Acknowledgements

This work was supported by ERC Advanced Grant RG.BIO (785932) to ACa, and ERANET-CRIB grant to ACa and TSG. TSG was also supported by grants from CONICET, ANPCyT and UNLP (Argentina). The authors acknowledge several illuminating discussions with William Bialek regarding speed control in flocks. ACu wishes to thank Victor Martin-Major for careful advice on the numerics. ACa warmly thanks Frank Heppner for reading the original manuscript and for a decade-long conversation on collective avian behaviour.

Author contributions

ACa, IG and TSG designed the study. XF, WKK, SM, LP, and PV - coordinated by SM - collected the experimental data. SM carried out the 3D dynamical tracking of the raw experimental data. ACa, ACu, and TSG performed the analytic calculation. ACu and GP carried out the numerical simulations. ACu analysed the experimental and numerical data. ACa and IG wrote the manuscript.

-
- [1] C. W. Reynolds, "Flocks, herds and schools: A distributed behavioral model," in *Proceedings of the 14th annual conference on Computer graphics and interactive techniques*, pp. 25–34, 1987.
 - [2] F. Heppner and U. Grenander, "A stochastic nonlinear model for coordinated bird flocks," *The ubiquity of chaos*, vol. 233, p. 238, 1990.
 - [3] A. Huth and C. Wissel, "The simulation of the movement of fish schools," *Journal of theoretical biology*, vol. 156, no. 3, pp. 365–385, 1992.
 - [4] T. Vicsek, A. Czirók, E. Ben-Jacob, I. Cohen, and O. Shochet, "Novel type of phase transition in a system of self-driven particles," *Phys Rev Lett*, vol. 75, pp. 1226–1229, Aug 1995.
 - [5] I. D. Couzin, J. Krause, R. James, G. D. Ruxton, and N. R. Franks, "Collective memory and spatial sorting in animal groups," *Journal of theoretical biology*, vol. 218, no. 1, pp. 1–11, 2002.
 - [6] H. Chaté, F. Ginelli, G. Grégoire, F. Peruani, and F. Raynaud, "Modeling collective motion: Variations on the vicsek model," *Eur. Phys. J. B*, vol. 64, pp. 451–456, 08 2008.
 - [7] P. Romanczuk and L. Schimansky-Geier, "Swarming and pattern formation due to selective attraction and repulsion," *Interface focus*, vol. 2, no. 6, pp. 746–756, 2012.
 - [8] R. Grossmann, L. Schimansky-Geier, and P. Romanczuk, "Self-propelled particles with selective attraction–repulsion interaction: from microscopic dynamics to coarse-grained theories," *New Journal of Physics*, vol. 15, no. 8, p. 085014, 2013.
 - [9] A. Perna, G. Grégoire, and R. P. Mann, "On the duality between interaction responses and mutual positions in flocking and schooling," *Movement ecology*, vol. 2, no. 1, pp. 1–11, 2014.
 - [10] A. Cavagna, A. Cimarelli, I. Giardina, G. Parisi, R. Santagati, F. Stefanini, and M. Viale, "Scale-free correlations in starling flocks," *Proc Natl Acad Sci USA*, vol. 107, pp. 11865–70, Jun 2010.
 - [11] J. M. Rayner, P. W. Viscardi, S. Ward, and J. R. Speakman, "Aerodynamics and energetics of intermittent flight in birds," *American Zoologist*, vol. 41, no. 2, pp. 188–204, 2001.
 - [12] W. Bialek, A. Cavagna, I. Giardina, T. Mora, O. Pohl, E. Silvestri, M. Viale, and A. M. Walczak, "Social interactions dominate speed control in poising natural flocks near criticality," *Proceedings of the National Academy of Sciences*, vol. 111, no. 20, pp. 7212–7217, 2014.
 - [13] C. K. Hemelrijk and H. Hildenbrandt, "Scale-free correlations, influential neighbours and speed control in flocks of birds," *Journal of Statistical Physics*, vol. 158, no. 3, pp. 563–578, 2015.
 - [14] C. K. Hemelrijk and H. Hildenbrandt, "Self-organized shape and frontal density of fish schools," *Ethology*, vol. 114, no. 3, pp. 245–254, 2008.
 - [15] D. Helbing and P. Molnár, "Social force model for pedestrian dynamics," *Phys. Rev. E*, vol. 51, pp. 4282–4286, May 1995.
 - [16] D. Helbing, I. Farkas, and T. Vicsek, "Simulating dynamical features of escape panic," *Nature*, vol. 407, pp. 487–490, September 2000.
 - [17] D. Helbing, I. Farkas, P. Molnar, and T. Vicsek, "Simulation of pedestrian crowds in normal and evacuation situations," vol. 21, pp. 21–58, 01 2002.
 - [18] A. Garrell, L. Garza-Elizondo, M. Villamizar, F. Herero, and A. Sanfeliu, "Aerial social force model: A new framework to accompany people using autonomous flying robots," in *2017 IEEE/RSJ International Conference on Intelligent Robots and Systems (IROS)*, pp. 7011–7017, 2017.
 - [19] D. Yang, U. Ozguner, and K. Redmill, "Social force based microscopic modeling of vehicle-crowd interaction," in *2018 IEEE Intelligent Vehicles Symposium (IV)*, pp. 1537–1542, 2018.
 - [20] A. Cavagna, I. Giardina, A. Orlandi, G. Parisi, A. Procaccini, M. Viale, and V. Zdravkovic, "The starflag handbook on collective animal behaviour: 1. empirical methods," *Anim Behav*, vol. 76, pp. 217–236, Jan 2008.
 - [21] A. Cavagna, I. Giardina, A. Orlandi, G. Parisi, and A. Procaccini, "The starflag handbook on collective animal behaviour: 2. three-dimensional analysis," *Anim Behav*, vol. 76, pp. 237–248, Jan 2008.
 - [22] A. Attanasi, A. Cavagna, L. Del Castello, I. Giardina, T. S. Grigera, A. Jelić, S. Melillo, L. Parisi, O. Pohl, E. Shen, *et al.*, "Information transfer and behavioural inertia in starling flocks," *Nature physics*, vol. 10, no. 9, pp. 691–696, 2014.
 - [23] J. Goldstone, "Field theories with superconductor solutions," *Il Nuovo Cimento (1955-1965)*, vol. 19, no. 1, pp. 154–164, 1961.
 - [24] A. Z. Patashinskii and V. L. Pokrovskii, *Fluctuation Theory of Phase Transitions*. Pergamon Press, 1979.
 - [25] T. Vicsek and A. Zafeiris, "Collective motion," *Physics*

- Reports*, vol. 517, no. 3, pp. 71–140, 2012.
- [26] F. Ginelli, “The physics of the Vicsek model,” *The European Physical Journal Special Topics*, vol. 225, no. 11-12, pp. 2099–2117, 2016.
 - [27] R. Zwanzig, *Nonequilibrium statistical mechanics*. Oxford University Press, USA, 2001.
 - [28] T. Mora, A. M. Walczak, L. Del Castello, F. Ginelli, S. Melillo, L. Parisi, M. Viale, A. Cavagna, and I. Giardina, “Local equilibrium in bird flocks,” *Nature Physics*, vol. 12, no. 12, pp. 1153–1157, 2016.
 - [29] M. Le Bellac, *Quantum and Statistical Field Theory*. Clarendon Press Oxford, 1991.
 - [30] N. Goldenfeld, *Lectures on Phase Transitions and the Renormalization Group*. Reading, Massachusetts: Perseus Books, 1992.
 - [31] J. J. Binney, N. Dowrick, A. Fisher, and M. Newman, *The theory of critical phenomena: an introduction to the renormalization group*. Oxford University Press, Inc., 1992.
 - [32] E. Brézin, D. Wallace, and K. G. Wilson, “Feynman-graph expansion for the equation of state near the critical point,” *Physical Review B*, vol. 7, no. 1, p. 232, 1973.
 - [33] E. Brézin and D. Wallace, “Critical behavior of a classical heisenberg ferromagnet with many degrees of freedom,” *Physical Review B*, vol. 7, no. 5, p. 1967, 1973.
 - [34] A. Patashinskii and V. Pokrovskii, “Longitudinal susceptibility and correlations in degenerate systems,” *Zh. Eksp. Teor. Fiz*, vol. 64, p. 1445, 1973.
 - [35] A. Cavagna, A. Culla, L. Di Carlo, I. Giardina, and T. S. Grigera, “Low-temperature marginal ferromagnetism explains anomalous scale-free correlations in natural flocks,” *Comptes Rendus Physique*, vol. 20, pp. 319–328, May-Jun 2019.
 - [36] W. J. Hamilton III, W. M. Gilbert, F. H. Heppner, and R. J. Planck, “Starling roost dispersal and a hypothetical mechanism regulating rhythmic animal movement to and from dispersal centers,” *Ecology*, vol. 48, no. 5, pp. 825–833, 1967.
 - [37] F. H. Heppner, “Avian flight formations,” *Bird-banding*, vol. 45, no. 2, pp. 160–169, 1974.
 - [38] I. L. Bajec and F. H. Heppner, “Organized flight in birds,” *Animal Behaviour*, vol. 78, no. 4, pp. 777–789, 2009.
 - [39] C. J. Pennycuik, “Mechanical constraints on the evolution of flight,” *Memoirs of the California Academy of Sciences*, vol. 8, pp. 83–98, 1986.
 - [40] J. M. Rayner, “Form and function in avian flight,” in *Current ornithology*, pp. 1–66, Springer, 1988.
 - [41] J. M. Rayner, “Biomechanical constraints on size in flying vertebrates,” in *Symposia of the Zoological Society of London*, no. 69, pp. 83–110, London: The Society, 1960-1999., 1996.
 - [42] A. Cavagna, C. Creato, L. Del Castello, I. Giardina, S. Melillo, L. Parisi, and M. Viale, “Error control in the set-up of stereo camera systems for 3d animal tracking,” *The European Physical Journal Special Topics*, vol. 224, no. 17, pp. 3211–3232, 2015.
 - [43] A. Attanasi, A. Cavagna, L. Del Castello, I. Giardina, A. Jelić, S. Melillo, L. Parisi, F. Pellacini, E. Shen, E. Silvestri, *et al.*, “Greta-a novel global and recursive tracking algorithm in three dimensions,” *IEEE transactions on pattern analysis and machine intelligence*, vol. 37, no. 12, pp. 2451–2463, 2015.
 - [44] R. Hartley and A. Zisserman, *Multiple view geometry in computer vision*. Cambridge University Press, 2004.
 - [45] A. Cavagna, I. Giardina, and T. S. Grigera, “The physics of flocking: Correlation as a compass from experiments to theory,” *Physics Reports*, vol. 728, pp. 1–62, 2018.
 - [46] D. C. Rapaport, *The art of molecular dynamics simulation*. Cambridge University Press, 2nd ed., 2004.
 - [47] M. Ballerini, N. Cabibbo, R. Candelier, A. Cavagna, E. Cisbani, I. Giardina, V. Lecomte, A. Orlandi, G. Parisi, A. Procaccini, *et al.*, “Interaction ruling animal collective behavior depends on topological rather than metric distance: Evidence from a field study,” *Proceedings of the national academy of sciences*, vol. 105, no. 4, pp. 1232–1237, 2008.
 - [48] W. Bialek, A. Cavagna, I. Giardina, T. Mora, E. Silvestri, M. Viale, and A. M. Walczak, “Statistical mechanics for natural flocks of birds,” *Proc Natl Acad Sci USA*, vol. 109, pp. 4786–91, Mar 2012.
 - [49] F. Dyson, “General theory of spin-wave interactions,” *Physical review*, vol. 102, no. 5, p. 1217, 1956.
 - [50] M. Ballerini, N. Cabibbo, R. Candelier, A. Cavagna, E. Cisbani, I. Giardina, A. Orlandi, G. Parisi, A. Procaccini, M. Viale, and V. Zdravkovic, “Empirical investigation of starling flocks: a benchmark study in collective animal behaviour,” *Anim Behav*, vol. 76, pp. 201–215, Jan 2008.
 - [51] T. Mora and W. Bialek, “Are biological systems poised at criticality?,” *J Stat Phys*, vol. 144, pp. 268–302, Jul 2011.

Supplementary Information

Distribution of the mean speed: linear speed control

In this section we describe how to derive the approximate mean speed distribution of Eq. (6) in the main text. The starting point is the pseudo-Hamiltonian with the Gaussian potential:

$$H(\{\mathbf{v}_i\}) = \frac{J}{2} \sum_{i,j} n_{ij} (\mathbf{v}_i - \mathbf{v}_j)^2 + g \sum_i (v_i - v_0)^2 \quad (\text{S1})$$

where all the sums are from 1 to the number of particles in the system N . We are dealing with an active system, hence the matrix $n_{ij} = n_{ij}(t)$ depends on time. However, it has been shown in [28] that, due to the large polarization of real flocks, the relaxation time scale of $n_{ij}(t)$ is significantly larger than that of the velocities, so that a quasi-equilibrium approach to the problem is reasonable; from now on we will then consider a time-independent n_{ij} . The validity of this approach is retrospectively confirmed by the remarkable agreement between the predictions of the approximate equilibrium theory derived here below, and the results from self propelled particles simulations, as displayed in Fig.2b and Fig.2d of the main text. In the context of quasi-equilibrium, we can assume a Boltzmann-like distribution for the velocities

$$P(\{\mathbf{v}_i\}) = \frac{1}{Z} \exp(-\beta H(\{\mathbf{v}_i\})) . \quad (\text{S2})$$

where $\beta = 1/T$ is the inverse temperature, and quantifies the degree of noise in the system. Our aim is now to marginalize (S2) to get a probability distribution for the mean speed (notice that, although the confining potential is Gaussian, it is so in the *speed*, i.e. the modulus of the velocity, $|\mathbf{v}_i|$, which is *not* a linear function of \mathbf{v}_i ; hence, the model is in fact not Gaussian). It is convenient to rewrite (S1) in terms of the individual speeds $v_i = |\mathbf{v}_i|$ and flight directions $\boldsymbol{\sigma}_i = \mathbf{v}_i/v_i$. In the very ordered phase, one can use the “spin-wave approximation” (SW) [49], as already done in previous analysis of starling flocks [12, 48]. When the polarization is large (enforced in our model by choosing $J \gg 1$), the flight direction of each individual is very close to the polarization vector. Hence:

$$\mathbf{v}_i = v_i \boldsymbol{\sigma}_i \quad \text{with} \quad |\boldsymbol{\sigma}_i| = 1 \quad (\text{S3})$$

$$\boldsymbol{\sigma}_i \simeq \mathbf{n} \left(1 - \frac{\pi_i^2}{2} \right) + \boldsymbol{\pi}_i \quad (\text{S4})$$

where \mathbf{n} is the unit vector along the polarization vector $\boldsymbol{\Phi} = \frac{1}{N} \sum_i \boldsymbol{\sigma}_i$, and the $\boldsymbol{\pi}_i$ are the fluctuations orthogonal to \mathbf{n} . The constraint $\sum_i \boldsymbol{\pi}_i = 0$ holds by construction and, in the high ordered regime, $\pi_i^2 \ll 1$ for every i . The Hamiltonian (S1) then becomes, up to order π_i^2 :

$$H(\{v_i\}, \{\boldsymbol{\pi}_i\}) = J \sum_{i,j} \Lambda_{ij} v_i v_j + g \sum_i (v_i - v_0)^2 + J \sum_{i,j} \tilde{\Lambda}_{ij}(\{v_k\}) \boldsymbol{\pi}_i \cdot \boldsymbol{\pi}_j , \quad (\text{S5})$$

where we defined the matrices:

$$\Lambda_{ij} = -n_{ij} + \delta_{ij} \sum_k n_{ik} \quad (\text{Discrete Laplacian}) \quad (\text{S6})$$

$$\tilde{\Lambda}_{ij}(\{v_k\}) = -n_{ij} v_i v_j + \delta_{ij} \sum_k n_{ik} v_i v_k \quad (\text{S7})$$

In terms of the variables $\{v_i\}$ and $\{\boldsymbol{\pi}_i\}$, the probability density (S2) becomes,

$$P(\{v_i\}, \{\boldsymbol{\pi}_i\}) = \frac{\delta \left(\sum_k \boldsymbol{\pi}_k \right) \prod_i v_i^{d-1} e^{-\beta H}}{\int Dv' D\boldsymbol{\pi}' \delta \left(\sum_k \boldsymbol{\pi}'_k \right) e^{-\beta H} \prod_i v_i'^{d-1}} \quad (\text{S8})$$

where $Dv' \equiv \prod_k dv'_k$, $D\boldsymbol{\pi}' \equiv \prod_k d\boldsymbol{\pi}'_k$ and d is the dimension of the velocity vector. We now need to integrate out the fluctuations $\boldsymbol{\pi}_i$, to obtain the marginalized distribution of the individual speeds v_i . Let us define

$$\Omega(\{v_i\}) \equiv \prod_j v_j^{d-1} \int D\boldsymbol{\pi} \exp \left[-\beta J \sum_{i,j} \tilde{\Lambda}_{ij}(\{v_k\}) \boldsymbol{\pi}_i \cdot \boldsymbol{\pi}_j \right] \delta \left(\sum_k \boldsymbol{\pi}_k \right) \quad (\text{S9})$$

The integral can be easily performed upon a change of integration variables from the $\{\pi_i\}$ to the eigenvectors $\{\tilde{\pi}_\alpha\}$ of the matrix $\tilde{\Lambda}$. Both Λ and $\tilde{\Lambda}$ inherit the translational invariance of the original Hamiltonian and have a constant eigenvector corresponding to a zero mode, since $\sum_j \Lambda_{ij} = \sum_j \tilde{\Lambda}_{ij} = 0$. The constraint on the $\{\pi_i\}$ becomes a constraint on the zero mode, i.e. $\delta(\tilde{\pi}_0)$, making the integral finite and leaving out only $d-1$ eigenvalues. We get

$$\Omega(\{v_i\}) = \left[\prod_j v_j^{d-1} \right] \left[\prod_{\alpha \neq 0} \tilde{\lambda}_\alpha(\{v_k\}) \right]^{-\frac{d-1}{2}} \quad (\text{S10})$$

where the $\{\tilde{\lambda}_\alpha\}$ are the eigenvalues of $\tilde{\Lambda}$ and depend on the $\{v_i\}$ in some complicated way. Since we are interested in the distribution of the mean speed $s = (1/N) \sum_i v_i$, we will now estimate the behaviour of Ω to leading order in s . Once again, it is convenient to make a change of variables, going from real space to the space of the eigenvectors $\{\hat{v}_a\}$ of the discrete Laplacian Λ . Each v_i can be decomposed into its \hat{v}_a components using the formula $v_i = \sum_a w_i^{(a)} \hat{v}_a$, where $w_i^{(a)}$ is the change of basis matrix. As mentioned above, the zero-mode has constant coefficients $w_i^{(0)} = 1/\sqrt{N}$ and the zero-mode eigenvector is therefore proportional to the mean speed, i.e. it is exactly $\sqrt{N}s = (1/\sqrt{N}) \sum_i v_i$. This also implies that for each v_i we have

$$v_i = s + \delta v_i = s + \sum_{a \neq 0} w_i^{(a)} \hat{v}_a. \quad (\text{S11})$$

We can now express the function Ω , in terms of this new representation

$$\Omega \sim \frac{\prod_j v_j^{d-1}}{\left[\prod_{\alpha \neq 0} \tilde{\lambda}_\alpha(\{v_k\}) \right]^{\frac{d-1}{2}}} = \frac{\prod_j \left[s + \sum_{a \neq 0} w_j^{(a)} \hat{v}_a \right]^{d-1}}{f \left(\left\{ s + \sum_{a \neq 0} w_k^{(a)} \hat{v}_a \right\} \right)} = s^{d-1} \frac{\prod_j \left[1 + \sum_{a \neq 0} \frac{w_j^{(a)} \hat{v}_a}{s} \right]^{d-1}}{f \left(\left\{ 1 + \sum_{a \neq 0} \frac{w_k^{(a)} \hat{v}_a}{s} \right\} \right)} = s^{d-1} h \left(\left\{ 1 + \sum_{a \neq 0} \frac{w_k^{(a)} \hat{v}_a}{s} \right\} \right). \quad (\text{S12})$$

Here h is a generic rational function of its argument. The function f is a generic polynomial of order $(N-1)(d-1)$ in its argument (from dimensional analysis), hence it is safe to extract a $s^{(N-1)(d-1)}$, because s is present in the expansion of every v_k .

The term Ω describes the contribution to the measure coming from the integration of the directional fluctuations. Once we integrate the directional fluctuations, we have an Hamiltonian that only depends on the moduli $\{v_i\}$. Also in this case, we can express everything in terms of s and the non-zero modes $\{\hat{v}_a\}$ of Λ . Remembering that $\sum_i w_i^{(a)} w_i^{(b)} = \delta_{a,b}$, we get:

$$H = J \sum_{i,j} \Lambda_{ij} v_i v_j + g \sum_i (v_i - v_0)^2 = \sum_{a=1}^N (J \lambda_a + g) \hat{v}_a^2 + gN(s - v_0)^2 \quad (\text{S13})$$

where, with a slight abuse of notation, we still indicate with H the marginalised Hamiltonian depending only on the speeds. After these manipulations we get the distribution

$$P(\{s, \hat{v}_a\}) = \frac{\Omega(\{s, \hat{v}_a\}) e^{-\beta H}}{\int ds' D\hat{v}' \Omega(\{s', \hat{v}'_b\}) e^{-\beta H}} \quad (\text{S14})$$

with $a \neq 0$ and $D\hat{v}' \equiv \prod_{b \neq 0} d\hat{v}'_b$. We can now derive the distribution of the mean speed $s = \frac{1}{N} \sum_i v_i$ by marginalizing over all the non-zero modes \hat{v}_a . To this end, we note that since $|w_i^{(a)}| < 1$ for every i and a , we have $\hat{v}_a = \sum_i w_i^{(a)} v_i < \sum_i v_i = Ns$. The domain of the variables appearing in (S14) is therefore:

$$0 \leq s < \infty \quad (\text{S15})$$

$$-Ns \leq \hat{v}_a \leq Ns \quad \text{for } a \neq 0 \quad (\text{S16})$$

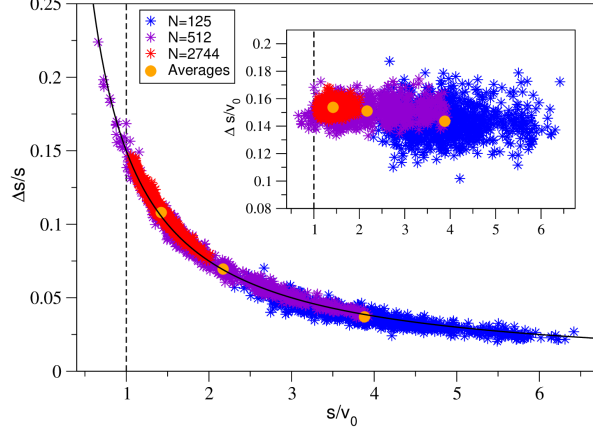


FIG. S1: **Relative fluctuations of the speed.** We report in this plot the relative fluctuations of the individual speed $\Delta s/s$ as a function of the mean speed, computed from numerical simulations for different values of N , and for $g = 10^{-3}$. The fluctuation is defined as $\Delta s = [(1/N) \sum_i \delta v_i^2]^{1/2}$. Each point in the plot corresponds to a distinct configuration, and all points of the same color are drawn from the same simulation performed at a given value of N . The big yellow points are averages over all data in the same simulation (i.e. N). The black line is a fit of the data with a $f(x) = a/x$ function. The vertical dashed line corresponds to $s = v_0$, which is the asymptotic value for the mean speed in the thermodynamic limit. The fluctuations themselves are small and depend on s only very weakly (inset), so that the *relative* fluctuations decay as $1/s$. Relative fluctuations therefore only increase due to the decrease of the average value of s at large sizes. However, such value is limited by below ($s < v_0$) and the relative fluctuations therefore remain small in the whole range of parameters.

We then get

$$\begin{aligned}
 P(s) &= \frac{1}{Z_s} \exp[-N\beta g(s - v_0)^2] \int_{-N^s}^{N^s} D\hat{v} \, \Omega(s, \{\hat{v}_a\}) \exp\left[-\beta \sum_{a=1}^N (J\lambda_a + g) \hat{v}_a^2\right] \\
 &= \frac{1}{Z_s} s^{d-1} \exp[-N\beta g(s - v_0)^2] \int_{-N^s}^{N^s} D\hat{v} \, h\left(\left\{1 + \sum_{a \neq 0} \frac{w_k^{(a)} \hat{v}_a}{s}\right\}\right) \exp\left[-\beta \sum_{a=1}^N (J\lambda_a + g) \hat{v}_a^2\right]
 \end{aligned} \tag{S17}$$

where Z_s is the normalization of the distribution and the integral in $D\hat{v}$ is over all the non-zero modes. We omitted all the irrelevant constants that cancel out through simplification between the distribution and its normalization. In the approximation where the relative fluctuations of the individual speeds are small, we can expand the function h appearing in the above expression and compute the remaining Gaussian integral for large values of N . We obtain, at leading order

$$P(s) = \frac{1}{Z} s^{d-1} \exp\left[-\frac{Ng}{T}(s - v_0)^2\right] \tag{S18}$$

We stress that the above approximation is quite reasonable in the deeply ordered phase. The quantity $\delta v_i = \sum_{a \neq 0} w_i^{(a)} \hat{v}_a$ indeed represents the fluctuation of the individual speed with respect to the mean speed of the group, s , and it must not be confused with the fluctuations of the mean speed itself. At low noise, when mutual adaptation is strong, individuals efficiently coordinate both their directions and speeds so that we expect individual deviations from the group mean flight direction (the polarization), and the mean speed to be small (as confirmed by simulations, see Fig. S1). On the other hand, if the value of g is small, i.e. the control on the individual speeds is loose, the $\{v_i\}$ can remain coordinated and at the same time wildly fluctuate (e.g. everyone speeds up), giving rise to large fluctuations of s , while keeping the relative deviations δv_i small.

The average value of the mean speed computed from distribution (S18) has been plotted in Fig.2b of the main paper: it predicts very nicely the values measured through numerical simulations of the off-lattice linear control model (see next section for details), confirming the validity of the approximations performed in the calculation (i.e. large directional order, quasi-equilibrium, small relative fluctuations of the speed). To get an analytical estimate of

the typical speed, we can compute the maximum of the distribution. By imposing $\frac{\partial P}{\partial s} = 0$ for $d = 3$, we obtain the following equation:

$$s_{typical}^2 - s_{typical}v_0 - \frac{T}{Ng} = 0 \quad (S19)$$

that gives us the expression for the maximum:

$$s_{typical} = v_0 \left[\frac{1}{2} + \frac{1}{2} \sqrt{1 + \frac{4T}{Ngv_0^2}} \right] \quad (S20)$$

This result confirms the idea that the mean speed is substantially different from v_0 for small N , if g is too small, as clearly shown in Fig.2b of the main paper.

We wish to draw the reader's attention on the fact that, despite the approximations we used to derive them (in particular the fixed network assumption), the analytical results of this section are in perfect agreement with numerical simulations performed by using an actual self-propelled particle model (see Fig.2b in the main text). This is not surprising, considering that in the deeply ordered flocking phase the time scale to reshuffle the interaction network is much larger than the time of local relaxation [28].

Bounds on the stiffness for linear speed control

We have seen in the main text that when the stiffness g is small enough, correlations are scale free. To understand how small is "small enough", we notice that in order to have scale-free correlations at all observed sizes, one needs $\xi_{sp} \gg L$ for each L , a condition that, together with (see main text),

$$\xi_{sp} = r_1 \left(\frac{Jn_c}{g} \right)^{1/2} \quad (S21)$$

leads to,

$$g \ll \frac{a}{L_{\max}^2} \quad (S22)$$

where L_{\max} is the size of the largest flock in the dataset and $a = r_1^2 Jn_c$ collects all size-independent quantities. When the stiffness is so small that (S22) holds, scale-free correlations over the entire range of L are reproduced.

On the other hand, we can quantify the conflict between control and correlation within the linear theory by setting a second bound on the speed stiffness g . From (S20) we see that, in order to have a typical flock's speed reasonably close to the natural reference value, v_0 , one must ensure that $T/(Ngv_0^2) \ll 1$ for all observed sizes; if we use the reasonable approximation $N \sim L^3/r_1^3$, where r_1 is the mean nearest neighbour distance, we obtain the condition,

$$g \gg \frac{b}{L_{\min}^3} \quad (S23)$$

where L_{\min} is the size of the smallest flock in the data-set, and where once again we have grouped into the parameter $b = r_1^3 T/v_0^2$ all size-independent constants. Once the spectrum of observed values of L is wide enough, the two bounds (S22) and (S23) *cannot* be satisfied both with one single value of the speed control stiffness g . The only way to reconcile linear speed control with the empirical observations would be to assume the existence of a tuning mechanism such that the speed stiffness g depends on the size L of the flock, in a way to satisfy the following condition,

$$\frac{b}{L^3} \ll g(L) \ll \frac{a}{L^2} \quad (S24)$$

This is a rather narrow strip for $g(L)$ to live in, so that a biological mechanism fulfilling (S24) would require some very tricky size-dependent fine-tuning. But even that could be insufficient: the two asymptotic inequalities in (S24) require the stiffness g to stay well clear of both boundaries, b/L^3 and a/L^2 , which for medium-small values of L becomes impossible to achieve.

Distribution of the mean speed: marginal speed control

Let us now consider the marginal speed control model, that has the pseudo-Hamiltonian:

$$H(\{\mathbf{v}_i\}) = \frac{J}{2} \sum_{i,j} n_{ij} (\mathbf{v}_i - \mathbf{v}_j)^2 + \frac{\lambda}{v_0^6} \sum_i (v_i^2 - v_0^2)^4 \quad (\text{S25})$$

We can follow a similar procedure as the one used for linear control, i.e. we apply the SW approximation to deal with directional fluctuations and we decompose in normal modes for the speed fluctuations. We end up with a distribution with the same structure as the one of (S14) with

$$H = \sum_{a=1}^N J \lambda_a \hat{v}_a^2 + \frac{\lambda}{v_0^6} \sum_i \left(\sum_{a,b} w_i^{(a)} w_i^{(b)} \hat{v}_a \hat{v}_b - v_0^2 \right)^4 \quad (\text{S26})$$

Integration over the non-zero modes with this effective Hamiltonian is clearly a hard task, due to the non-Gaussian contributions. However, in the approximation where the relative speed fluctuations are small, things simplify: we can easily extract the zero mode contribution $\simeq N \frac{\lambda}{v_0^6} (s^2 - v_0^2)^4$ in the exponent, while at leading order the integration over the remaining modes (which is non Gaussian in this case) will produce a constant integral. The distribution for the average speed s will then be:

$$P(s) = \frac{1}{Z} s^{d-1} \exp \left[-\frac{N\lambda}{T v_0^6} (s^2 - v_0^2)^4 \right] \quad (\text{S27})$$

The agreement between theory and simulations is less accurate than in the linear speed control case, but we still have a satisfying match between the predicted average mean speed and the value measured from numerical simulations (Fig.2d of the main paper). Once again we can compute the maximum of the distribution to estimate the typical mean speed. For $d = 3$ we get:

$$1 - \frac{4N\lambda v_0^2}{T} \left(\frac{s_{\text{typical}}}{v_0} \right)^2 \left(\left(\frac{s_{\text{typical}}}{v_0} \right)^2 - 1 \right)^3 = 0 \quad (\text{S28})$$

Since we are interested in the behaviour of s_{typical} in N at fixed T and λ , we can solve this equation in the two limits of big N and small N , obtaining:

$$s_{\text{typical}} \simeq \begin{cases} v_0 \left[1 + \left(\frac{T}{32N\lambda v_0^2} \right)^{1/3} \right] & \text{for } N \gg \frac{T}{\lambda v_0^2} \\ v_0 \left(\frac{T}{4N\lambda v_0^2} \right)^{1/8} & \text{for } N \ll \frac{T}{\lambda v_0^2} \end{cases} \quad (\text{S29})$$

Polarization dependence on model parameters

In equilibrium ferromagnetic models in their low temperature phase, the polarization Φ only depends on the ratio between ferromagnetic coupling J and temperature T through the relation [49],

$$\Phi = 1 - \alpha \frac{T}{J} \quad (\text{S30})$$

where α is a constant of order 1 whose value depends on the specific structure of the interaction network. This relation, though, is only valid when the vectorial degrees of freedom \mathbf{v}_i have modulus 1, whereas if they have modulus equal to v_0 the relation changes to,

$$\Phi = 1 - \alpha \frac{T}{v_0^2 J} \quad (\text{S31})$$

For out-of-equilibrium models, as the present case, the polarization depends in principle on all parameters; however, in the deeply ordered phase that we are considering here, the main contribution to Φ is still given by the ratio between alignment and noise, so that (S31) remains a very useful rule of thumb to fix the parameters of the model such to have a polarization equal to that of natural flocks, namely $\Phi \simeq 0.89 \div 0.99$.

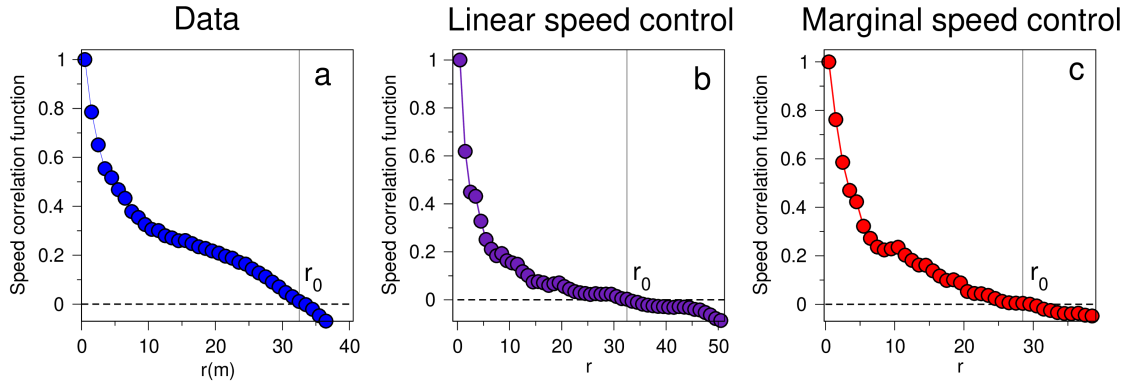


FIG. S2: **Some examples of connected correlation functions.** We report some examples of speed connected correlation functions, computed by eq. (11) of the main text. The first point of zero-crossing (r_0) is visible for each function. All the functions are normalized such that $C(r=0) = 1$. **a:** Example of speed connected correlation function in experimental data. **b:** Example of speed connected correlation function in linear speed control model simulations. **c:** Example of speed connected correlation function in marginal speed control model simulations. For **b** and **c** the distance r is measured in simulation units.

Gauging the values of N and L in numerical Simulations

In order to compare numerical data with experimental ones, we need to satisfy two criteria in our simulations: we must span a range in group sizes N analogous to the one of real flocks (to reproduce the behaviour of the mean speed as a function of N), and we also need to span a range in linear sizes L of the same order of what found in experiments (to reproduce the scaling of the correlation length). However, natural flocks have non-trivial aspect ratios (being flatter in the direction of gravity [50]), which implies that their spatial extension L^{bio} (defined as the maximum distance between two individuals) does not scale with the group size N^{bio} as $L^{\text{bio}} = (N^{\text{bio}})^{1/3}$. For this reason, we need to perform two sets of simulations to satisfy the criteria mentioned above. In the first set, we perform simulations with $N = 8 \div 2744$, that are the minimum and maximum number of individuals in the recorded natural flocks. With these numerical data we compute the mean speed distribution and its average, that are then displayed in Fig.2b,d. Then, we perform a second set of simulations with L/r_1 up to the maximum experimental value of $L^{\text{bio}}/r_1^{\text{bio}} = 70$, where r_1^{bio} is the average nearest neighbour distance of real flocks. With these data we compute the correlation lengths that are plotted in Fig.2a,c; for this set of simulations we have $N = 125 \div 343 \times 10^3$. An alternative strategy would have been to perform simulations in a box reproducing the aspect ratio of natural flocks, rather than in a cubic box. This is however not convenient. The aspect ratio for real flocks is not a stable quantity, but fluctuates from flock to flock and - for the same flock - from time to time. This would require an extremely painful calibration of the chosen simulation box. On the other hand, analysis of real data show that the aspect ratio does not influence the statistics of speeds and correlations (e.g. correlations of flocks with different aspect ratios rescale very well, safe for boundary effects at very large distances [10]). Choosing a cubic a box is therefore perfectly legitimate in terms of the physics, and it very much simplifies the data analysis.

Is the marginal theory tuned at criticality?

An interesting question is whether or not a theory with marginal speed control requires any tuning of the parameters, and in particular tuning close to criticality [51]. The success of the marginal theory is based on the fact that the second derivative of the potential is exactly zero at v_0 , a condition that seems to require some tuning. However, a small non-zero quadratic term would still be acceptable in the marginal case, as long as its amplitude is much smaller than $1/L_{\text{max}}^2$; and thanks to the steep nonlinear rise of the marginal potential, there is no lower bound for it, so that this tuning is therefore rather lukewarm. On the other hand, the marginal theory requires the system to be close to the zero-temperature critical point, so in this sense there is a case for near-criticality. However, a zero-temperature critical point is not shifted by finite-size effects, it has just one physical side (positive temperature); hence, we can just push the system at low temperature, without worrying to *cross* the critical point in any way; as a result, the control parameter does not need to depend on size to keep the system close to criticality. As we have seen, the situation would be different in the case of linear control, as the speed stiffness must be carefully tuned in a size-dependent way to remain close, but not too close, to the critical point.

Acquisition	No. of birds N	Flock's size L, m	Polarization Φ	Mean speed $s, m/s$	Correlation length ξ, m
16-05	1548	68.1	0.961	15.5	9.1
17-06	380	40.5	0.935	10.0	5.8
21-06	530	26.6	0.973	11.0	3.8
25-08	1079	52.5	0.962	12.7	7.1
25-10	696	30.1	0.991	12.6	3.3
25-11	854	33.1	0.957	10.7	3.4
28-10	1122	32.3	0.982	11.2	3.2
29-03	422	28.1	0.963	10.8	3.7
31-01	1565	67.3	0.921	7.5	8.5
32-06	690	18.4	0.981	10.0	2.6
42-03	366	27.2	0.979	10.2	3.4
48-17	709	25.7	0.886	13.5	3.0
49-05	636	15.1	0.995	13.7	2.0
54-08	2548	66.6	0.971	14.2	8.9
57-03	2559	76.1	0.978	14.3	10.7
58-06	351	19.4	0.987	10.8	2.2
58-07	445	15.3	0.977	10.9	2.4
63-05	712	47.2	0.978	10.3	4.1
69-09	206	13.4	0.985	11.8	1.8
69-10	994	32.4	0.987	12.0	4.1
69-13	1238	39.2	0.937	10.1	5.9
69-19	617	21.0	0.975	14.3	3.6
72-02	101	7.2	0.993	13.3	1.5
77-07	131	6.5	0.978	9.2	1.5
20110208_ACQ3	178	12.9	0.983	8.8	1.7
20110211_ACQ1	595	23.5	0.971	8.6	2.6
20110217_ACQ2	405	15.0	0.982	11.1	2.0
20111124_ACQ1	125	8.1	0.993	11.0	1.5
20111125_ACQ1	50	8.7	0.983	12.4	2.0
20111125_ACQ2	512	26.6	0.956	9.4	3.3
20111201_ACQ3.F1	133	8.2	0.973	10.2	1.0
20111201_ACQ3.F4	488	16.2	0.972	10.6	1.0
20111207_ACQ1	108	13.8	0.931	8.1	2.3
20111214_ACQ4.F1	154	10.3	0.992	11.4	1.8
20111214_ACQ4.F2	144	13.4	0.968	11.6	2.2
20111215_ACQ1	391	16.1	0.984	11.1	2.5
20111220_ACQ2	198	10.2	0.985	16.6	1.2
20191209_ACQ53	97	9.9	0.991	11.1	1.4
20191209_ACQ55.F1	19	5.6	0.996	13.3	1.3
20191209_ACQ58.F2	53	10.5	0.988	13.2	1.3
20191209_ACQ58.F3	14	1.5	0.998	17.2	1.6
20200129_ACQ3	54	10.1	0.998	17.4	1.1
20200129_ACQ4.F1	11	4.7	0.988	11.8	1.5
20200129_ACQ4.F2	54	13.2	0.994	16.6	1.5
20200211_ACQ7	10	1.2	0.995	12.0	0.8

TABLE I: **Experimental data.** This table reports all the data required to perform the analysis presented in this paper. Each line corresponds to a different acquisition (i.e. flocking recording), for all the three experimental campaigns considered (acquisitions labeling system changed from one campaign to another). Acquisitions belonging to different campaigns are separated by a straight line. For each acquisition we have: the median number of individuals N , the median flock's size L , the mean polarization $\Phi = 1/N \sum_i \mathbf{v}_i / v_i$, the median of the mean speed $s = 1/N \sum_i v_i$ and the median correlation length ξ , computed via eq. (13) of the main text (Methods). Every median (or mean), relative to a particular acquisition, is made over all the frames in that recording. Since the measured polarization value depends on time resolution (higher resolution bringing more noise), acquisition of the second and third campaign (that are acquired at much faster rates) have been re-sampled at the same rate of the first campaign so as to have homogeneous measurements for all the data.

Speed control	g	λ	T	J
Linear	0.001	-	2.5×10^{-3}	10
	0.03	-	2.5×10^{-3}	10
	0.1	-	2.5×10^{-3}	10
	1.0	-	2.5×10^{-3}	10
Marginal	-	0.001	1.25×10^{-4}	1.0

TABLE II: **Parameters of simulations.** In this table we report the values of relevant parameters used in the numerical simulations. The other parameters are $r_c = 1.2$, $v_0 = 0.05$, $\Delta t_{MRG} = 0.01$, $\Delta t_{GAUSS} = 0.001$.